A DISCRETE-TIME ROBUST STATE DERIVATIVE FEEDBACK CONTROLLER FOR AN ACTIVE SUSPENSION SYSTEM

FERNANDA QUELHO ROSSI*, ROBERTO KAWAKAMI HARROP GALVÃO*, DIOGO RAMALHO DE OLIVEIRA†, MARCELO CARVALHO MINHOTO TEIXEIRA†, EDVALDO ASSUNÇÃO†

*Praça Marechal Eduardo Gomes, 50, CEP 12228-900
Divisão de Engenharia Eletrônica, ITA - Instituto Tecnológico de Aeronáutica
São José dos Campos, SP, Brazil

†Av. José Carlos Rossi, 1370, CEP 15835-000
Departamento de Engenharia Elétrica, UNESP - Universidade Estadual Paulista
Ilha Solteira, SP, Brazil

Emails: fer.qrossi@gmail.com, kawakami@ita.br, diogo.ramalho@ifms.edu.br, marcelo@dee.feis.unesp.br, edvaldo@dee.feis.unesp.br

Abstract— This work presents the design and the experimental implementation of a robust state derivative feedback (SDF) controller in an active suspension system manufactured by Quanser® (Quanser, 2009a). For this purpose, a discrete-time SDF controller is designed in the presence of parametric uncertainties by using a state derivative model within a regional pole placement approach. In the implementations, only the measurements from accelerometers are employed, a typical motivation for the use of SDF. The dynamic behavior of the active suspension system is tested for different values of the uncertain parameter within its range considered in the controller design.

Keywords— state derivative feedback, discrete-time control, polytopic uncertainty, active suspension system

Resumo— Este trabalho apresenta o projeto e a implementação experimental de um controlador robusto usando realimentação da derivada dos estados em um sistema de suspensão ativa fabricado por Quanser® (Quanser, 2009a). Para este propósito, um controlador em tempo discreto com realimentação derivativa é projetado na presença de incertezas paramétricas usando um modelo baseado nas derivadas dos estados em um método de alocação regional de polos. Na implementação, emprega-se apenas medidas de acelerômetros, uma motivação típica para o uso de realimentação derivativa. O comportamento dinâmico do sistema de suspensão ativa é apresentado para diferentes valores da incerteza paramétrica dentro da faixa considerada no projeto.

Palavras-chave— realimentação da derivada dos estados, controle a tempo discreto, incerteza politópica, sistema de suspensão ativa

1 Introduction

Engineering applications have widely employed accelerometer as the main sensor in the instrumentation sets, due to the low operational cost, simple structure and the ease in measuring the acceleration signals, instead of displacement and velocity, in the absence of an absolute position reference (Yang et al., 1991). Examples of applications include active suspension devices (Reithmeier and Leitmann, 2003), (da Silva et al., 2013), vibration suppression of mechanical systems (Abdelaziz, 2012), driving assistance controllers (Fallah et al., 2013), vibration control of bridge cables (Duan et al., 2005), and earthquake hazard mitigation (Yang et al., 1991).

As the state variables of these systems usually correspond to displacements and velocities, the use of accelerometers has motivated a significant research in the control literature concerning state derivative feedback (SDF). In fact, by double integration of the measured accelerations, the estimated displacements may not have good accuracy, due to the propagation of errors associated to bias in the measurements (Abdelaziz, 2012) and uncertainty in the initial conditions for the integrators (Reithmeier and Leitmann, 2003). Thus, the use of SDF may be more convenient, since it employs velocities and accelerations, not displacements.

Most works concerning SDF design have been devoted to continuous-time controllers, such as pole placement in (Abdelaziz and Valášek, 2004), (Faria et al., 2009), linear quadratic regulators (LQR) in (Duan et al., 2005), (Faria et al., 2009), (Tseng and Hsieh, 2013), robust controllers formulation using linear matrix inequalities (LMIs) in (Assunção et al., 2007), (Faria et al., 2010), (da Silva et al., 2012), among others.

The discrete-time design of SDF controllers were still only developed in a few works. In (Cardim et al., 2009) and (Rossi et al., 2013), the design of SDF controllers in nominal equivalence to a given state feedback controller were presented. A direct discrete-time design of robust SDF control laws was proposed in (Rossi et al., 2018), dispensing with the need for a preliminary state feedback design. Moreover, this method allowed the design of controllers with robustness to parametric uncertainties. However, an experimental validation of this proposed technique was not exhibited in (Rossi et al., 2018), only numerical simulation results were shown.

In this context, this work presents a practical implementation of a robust discrete-time SDF controller designed by using the method proposed in (Rossi et al., 2018). This controller is applied to an active suspension system manufactured by Quanser® (Quanser, 2009a). For this purpose, a state derivative model is employed, as proposed in (Rossi et al., 2018), within a classic LMI approach for regional pole placement (Chilali and Gahinet, 1996). A robust SDF controller is then designed in the presence of parametric uncertainties (an uncertain mass of the system) and implemented using only measurements from accelerometers.

The remainder of this paper is organized as follows. Section 2 describes the discrete-time design of controllers using SDF proposed in (Rossi et al., 2018). Section 3 presents the active suspension system. The controller design is developed in Section 4 and the practical implementation and results are exhibited in Section 5. Finally, concluding remarks are shown in Section 6.

2 State derivative feedback in discrete-time controllers design

The method proposed in (Rossi et al., 2018) for discrete-time controller design using SDF is presented in this section.

Consider a system described by a continuous-time model of the form

$$\dot{x}(t) = \Phi_c x(t) + \Gamma_c u(t) \tag{1}$$

with the state vector $x(t) \in \mathbb{R}^n$, the control input $u(t) \in \mathbb{R}^m$, and the constant matrices $\Phi_c \in \mathbb{R}^{n\times n}$, $\Gamma_c \in \mathbb{R}^{n\times m}$, with Φ_c non-singular.

Assume that the system is to be controlled by using sampled measurements of the state derivative $\dot{x}(kT)$, $k \in \mathbb{Z}$, where T is the sampling period. Moreover, consider that a zero order hold is employed to keep the control $u(t)$ constant between sampling times, i.e.

$$u(t) = u(kT)^+, \;\; (kT)^+ \le t \le (k+1)T \tag{2}$$

The superscript + in (2) is employed to indicate that the control is updated immediately after the state derivative is measured at each sampling time. Therefore, the state derivative of the system (1) at time $t = kT$ is given by

$$\dot{x}(kT) = \Phi_c x(kT) + \Gamma_c u((k-1)T)^+ \tag{3}$$

Since the control is kept constant between sampling times, as in Eq. (2), the model (1) can be discretized as

$$x((k+1)T) = \Phi x(kT) + \Gamma u(kT)^+ \tag{4}$$

with $\Phi = e^{\Phi_c T}$ and $\Gamma = \int_0^T e^{\Phi_c \tau}\Gamma_c \,\mathrm{d}\tau$.

The following theorem shows that the model (4) can be reformulated in terms of the derivative of the state $\dot{x}(kT)$ and the control input, in a suitable form for use in discrete-time control design.

Theorem 1 *Let $\dot{x}(kT)$ denote the derivative of the state at sampling time $t = kT$, immediately before the control update. The discrete-time model (4) can then be recast into the following form:*

$$\xi((k+1)T) = A\xi(kT) + Bu(kT)^+ \tag{5}$$

with $\xi(kT) \in \mathbb{R}^{n+m}$, $A \in \mathbb{R}^{(n+m)\times(n+m)}$ and $B \in \mathbb{R}^{(n+m)\times m}$ defined as

$$\xi(kT) \triangleq \begin{bmatrix} \dot{x}(kT) \\ u((k-1)T)^+ \end{bmatrix} \tag{6}$$

$$A = \begin{bmatrix} \Phi & -\Phi\Gamma_c \\ 0 & 0 \end{bmatrix}, \quad B = \begin{bmatrix} \Phi\Gamma_c \\ I \end{bmatrix} \tag{7}$$

where 0 and I denote a matrix of zeros and an identity matrix of appropriate dimensions, respectively.

Proof: See in (Rossi et al., 2018). □

Remark 1 *The representation (5) derived in Theorem 1 can be employed to design control laws of the form:*

$$u(kT)^+ = F\xi(kT) \tag{8}$$

with a feedback gain matrix $F \in \mathbb{R}^{m\times(n+m)}$, which can be designed through standard discrete-time state-space methods. In the examples illustrated in Section 5, it is assumed that the control task starts at time $k = 0$ and thus the control law is initialized with $u(-T)^+ = 0$.

Remark 2 (Polytopic uncertainties) *Consider a model of the form (1), with matrices Φ_c and Γ_c subject to polytopic uncertainties, i.e. $(\Phi_c, \Gamma_c) \in \Omega_{\Phi_c,\Gamma_c}$, where Ω_{Φ_c,Γ_c} is a polytope with known vertices $(\Phi_{c,i}, \Gamma_{c,i})$, $i = 1, 2, \ldots, N$. In addition, let $\Phi_i = e^{\Phi_{c,i}T}$ and assume that the sampling period T is sufficiently small so that the quadratic and higher-order terms in the power series expansion of $e^{\Phi_{c,i}T}$ can be neglected in the uncertainty representation. Therefore, the matrices (Φ, Γ_c) will lie in a polytope Ω_{Φ,Γ_c} with vertices $(\Phi_i, \Gamma_{c,i})$, $i = 1, 2, \ldots, N$. Thus, in view of the product between Φ and Γ_c in (7), the (A, B) matrices in (5) will belong to a polytope with N^2 vertices, which are associated to the cross-products between the vertices Φ_i, $i = 1,2,\ldots,N$, and $\Gamma_{c,j}$, $j = 1,2,\ldots,N$. In cases where T is not sufficiently small for assuming the hypothesis considered above, this issue needs to be studied in more detail. Indeed, in these cases, the use of techniques for the systematic treatment of the high order terms in the discretization procedure could be investigated, as proposed in (Braga et al., 2014). However, the first approach described herein leads to simpler design procedures and can be appropriate to meet closed-loop specifications, as will be illustrated in Section 5.*

3 Active suspension system

Fig. 1 shows the active suspension plant at Laboratório de Pesquisa em Controle (LPC), Faculdade de Engenharia de Ilha Solteira / Universidade Estadual Paulista "Júlio de Mesquita Filho" (FEIS/UNESP), where the experiments reported herein were carried out. It is a bench-scale model representing a classic quarter-car model controlled by an active suspension mechanism. This plant consists of three floors/plates on top of each other. The top floor (blue plate) represents the vehicle body supported above the suspension. The middle floor (red plate) corresponds to the tire. The bottom floor (silver plate) provides the road excitation in the system. A DC motor is standing between the top and middle floors to emulate an active suspension system.

A schematic model is represented in Fig. 2. The sprung mass M_s represents the mass of the vehicle body. The unsprung mass M_{us} represents the vehicle tire set. The spring k_s and the damper b_s support the body weight over the tire. The spring k_{us} and the damper b_{us} model the stiffness of the tire in contact with the road. The force F_c controls the motor (actuator) connected between the masses M_s and M_{us}, which represents the active suspension mechanism used to reduce the vibrations caused by chances on the bottom floor z_r. The control actuator F_c is limited to work in the range $-39.5\text{ N} \leq F_c \leq 39.5\text{ N}$.

The system dynamics can be described by a continuous-time state equation of the form (Quanser, 2009a):

$$\dot{x}(t) = \Phi_c x(t) + \Gamma_c u(t) + \Gamma_{c,d}\, u_d(t) \tag{9}$$

with

$$x(t) = \begin{bmatrix} z_s(t) - z_{us}(t) \\ \dot{z}_s(t) \\ z_{us}(t) - z_r(t) \\ \dot{z}_{us}(t) \end{bmatrix} \tag{10}$$

$$u(t) = F_c, \quad u_d(t) = \dot{z}_r(t) \tag{11}$$

$$\Phi_c = \begin{bmatrix} 0 & 1 & 0 & -1 \\ -\frac{k_s}{M_s} & -\frac{b_s}{M_s} & 0 & \frac{b_s}{M_s} \\ 0 & 0 & 0 & 1 \\ \frac{k_s}{M_{us}} & \frac{b_s}{M_{us}} & -\frac{k_{us}}{M_{us}} & -\frac{b_s+b_{us}}{M_{us}} \end{bmatrix} \tag{12}$$

$$\Gamma_c = \begin{bmatrix} 0 \\ \frac{1}{M_s} \\ 0 \\ -\frac{1}{M_{us}} \end{bmatrix}, \quad \Gamma_{c,d} = \begin{bmatrix} 0 \\ 0 \\ -1 \\ \frac{b_{us}}{M_{us}} \end{bmatrix} \tag{13}$$

where z_s and z_{us} denote the vertical displacements of masses M_s and M_{us}, respectively, and $\dot{z}_s$ and $\dot{z}_{us}$ represent the corresponding velocities. The first state represents the suspension deflection. The third state represents the tire deflection. The control input u is composed by the force F_c. The input u_d is the bottom floor excitation represented by its velocity $\dot{z}_r$. The system parameters are $M_s = 2.45$ kg, $M_{us} = 1$ kg, $k_s = 900$ N/m, $k_{us} = 2500$ N/m, $b_s = 7.5$ Ns/m and $b_{us} = 5$ Ns/m.

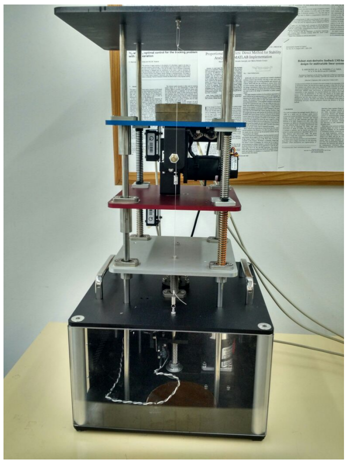

Figure 1: Active suspension system at LPC, FEIS/UNESP.

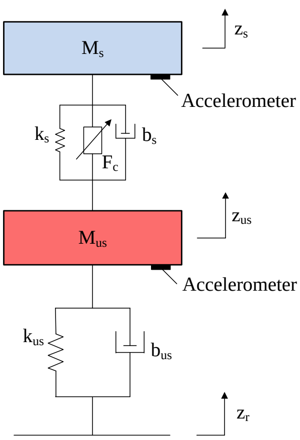

Figure 2: Schematic model of the active suspension system represented by double mass-spring-damper.

In the system, there is a payload mass (brass) removable in the vehicle body mass M_s. It consists of two identical weight units, each one weighting 0.4975 kg. The M_s value corresponds to the total mass ($M_s = 2.45$ kg), which includes the total payload mass. Without the payload mass, $M_s = 1.455$ kg. Therefore, the M_s mass may be uncertain in a range of $1.455\text{ kg} \leq M_s \leq 2.45$ kg (without or with the two weight units).

This active suspension system has two accelerometers measuring the accelerations $\ddot{z}_s(kT)$ and $\ddot{z}_{us}(kT)$ of the masses M_s and M_{us}, respectively. The velocities $\dot{z}_s(kT)$ and $\dot{z}_{us}(kT)$ can be estimated by integration of the respective acceleration signals. Moreover, the motion of the bottom plate (z_r) and the middle plate (z_{us}) is tracked by two encoders. A third encoder measures the motion of the top plate relative to the middle one ($z_s - z_{us}$). However, these signals from the encoders will not be used in the control system, they will only be used to register the results.

It is worth mentioning that the original active suspension system from Quanser® does not have an accelerometer to measure $\ddot{z}_{us}(t)$. For implementation of SDF, the addition of this accelerometer to the system was requested by the researchers from LPC, for the manufacturer.

4 Controller design

In order to decrease the oscillations caused by changes on the bottom floor z_r, a regulator control system was designed for the active suspension system. Since the acceleration signals of the system were measured and the mass M_s was subject to uncertainties, an SDF control law in the presence of parametric uncertainties was developed. For this purpose, the state derivative representation (5) proposed in Theorem 1 was employed within the classic LMI approach for regional pole placement presented in (Chilali and Gahinet, 1996) (see Appendix A).

In the experimental tests that will be performed, z_r is piecewise constant. In the time interval where z_r is constant, $\dot{z}_r$ is zero, while during the changes on the bottom floor z_r from a constant value to another, $\dot{z}_r$ is different from zero. However, a change occurs in a small time interval. Therefore, the motion of z_r is considered fast enough so that the transient response of the signal z_r can be disregarded in the analysis. Then, in each part where the control regulation will be carried out, $\dot{z}_r$ is considered zero.

By considering $\dot{z}_r = 0$, the model (9) can be described by a state equation of the form (1), with $x(kT)$, Φ_c, Γ_c as in (10), (12), (13) respectively. As the M_s mass is uncertain in a range of 1.455 kg $\leq M_s \leq$ 2.45 kg, the model is of the form (1) with $(\Phi_c, \Gamma_c) \in Co\{(\Phi_{c,1}, \Gamma_{c,1}), (\Phi_{c,2}, \Gamma_{c,2})\}$, where $M_s = 1.455$ kg (without payload mass) for $(\Phi_{c,1}, \Gamma_{c,1})$ and $M_s = 2.45$ kg (with total payload mass) for $(\Phi_{c,2}, \Gamma_{c,2})$.

Table 1 presents the eigenvalues of matrices $\Phi_{c,1}$ and $\Phi_{c,2}$, as well as the corresponding damping ratios (ζ), natural frequencies (ω_n) and natural oscillation periods $T_n = 2\pi/\omega_n$. As can be observed, the plant has two 2nd-order modes, with dynamics features that depend on the uncertain mass M_s. For discrete-time control purposes, it was employed the default sampling period adopted in the software package provided by Quanser®, $T = 1$ ms, which is 100 times smaller than the smallest T_n value, as shown in Table 1.

Table 1: Eigenvalues of the continuous-time model vertices, with corresponding damping ratios (ζ), natural frequencies (ω_n) and natural oscillation periods $T_n = 2\pi/\omega_n$.

	Eigenvalues	ζ	$\omega_n(rad/s)$	$T_n(s)$
$\Phi_{c,1}$	$-7.50 \pm j59.3$	0.12	59.8	0.10
	$-1.33 \pm j20.8$	0.06	20.8	0.30
$\Phi_{c,2}$	$-6.95 \pm j58.7$	0.12	59.1	0.11
	$-0.83 \pm j16.2$	0.05	16.2	0.40

In light of Theorem 1, the resulting discrete-time plant model can be cast into the form (5), with A, B as in (7) and

$$\xi(kT) = \begin{bmatrix} \dot{z}_s(kT) - \dot{z}_{us}(kT) \\ \ddot{z}_s(kT) \\ \dot{z}_{us}(kT) \\ \ddot{z}_{us}(kT) \\ u((k-1)T)^+ \end{bmatrix} \tag{14}$$

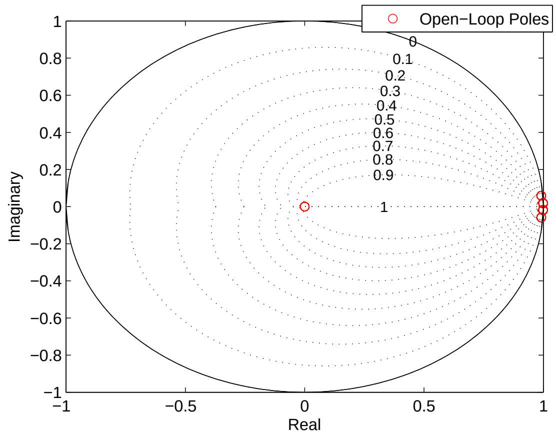

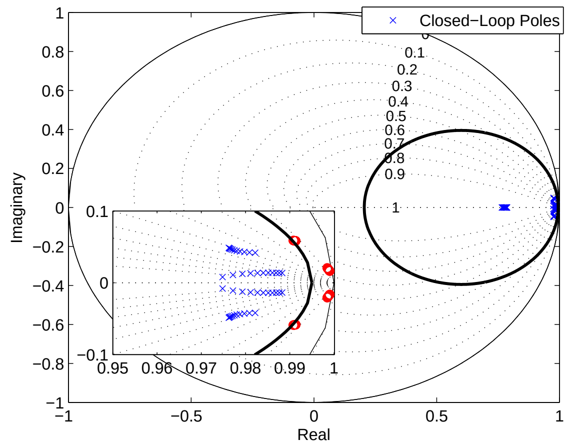

Figure 3: (a) Open-loop poles of the state derivative model for the active suspension system. The dotted lines correspond to curves of constant damping ratio ζ. (b) Closed-loop poles, with the boundary of the allocation region indicated as a thick line. The open-loop and closed-loop poles in the proximity of the unit circle are shown as inset.

Fig. 3a presents the open-loop poles of the discrete-time model (i.e. the eigenvalues of A), obtained by varying the parameter M_s in the range $1.455 \leq M_s \leq 2.45$ kg. It is worth noting that there is a pole at the origin for each case, which is associated to the row of zeros for the past control input in the structure of A defined in (7).

The control problem considered herein consists of designing a control law of the form (8), so that the closed-loop poles are placed in a desired region for any value of the uncertain parameter M_s. For stability in discrete-time, the conventional desired location of the eigenvalues is inside the unit circle in the complex plane. However, for a better transient behavior of the system, a more restricted region inside the unit circle may be selected for pole placement, in order to include performance constraints. For this purpose, in this work, the allocation region was chosen as a circle of radius $r = 0.395$ centered at (0.6, 0) (depicted as a thick line in Fig. 3b). More details about the choice of the allocation region can be found at (Rossi, 2018).

The gain matrix F was then obtained by using the LMI approach of (Chilali and Gahinet, 1996) described in Appendix A, with $\xi(kT)$, A, B in place of $x(kT)$, Φ, Γ, respectively. As can be seen in the plant dynamics described in (12)-(13), the uncertainty in the parameter M_s affects both Φ_c and Γ_c. Therefore, as discussed in Remark 2, the (A, B) matrices belong to a polytope with $N^2 = 4$ vertices formed from the pairwise combinations of Φ_1, Φ_2 and $\Gamma_{c,1}$, $\Gamma_{c,2}$. A feasible solution to the LMIs involved in the pole placement problem was obtained by using the Robust Control Toolbox^{TM} function "$feasp$", resulting in the following gain F:

$$F = \begin{bmatrix} -15.296 & -0.109 & -10.331 & -0.011 & 0.779 \end{bmatrix} \quad (15)$$

Fig. 3b shows the closed-loop poles (eigenvalues of $A + BF$), again obtained by varying the parameters M_s in the range of $1.455 \leq M_s \leq 2.45$ kg. An extended view of the open-loop and closed-loop poles in the proximity of the unit circle are shown as an inset, for a better visualization. A comparison with Fig. 3a reveals that the closed-loop poles are indeed with larger damping ratios ζ, aiming at a suppression of the oscillations.

5 Practical Implementations and Results

For experimental implementations in the active suspension system, the Matlab®/ Simulink® Software is connected to Quanser®'s QUARC® Real-Time Control Software, which enables the real-time control application directly from Simulink-designed controllers. The velocities and accelerations signals were used for feedback. The acceleration signals were measured by accelerometers and filtered, in order to remove bias and high frequency noises, employing filters adopted in the software package provided by Quanser®. The velocities were estimated by using suitable integrating filters developed at LPC.

As an excitation signal, z_r(t) was adopted to produce a square wave signal, with amplitude 0.02m, frequency of 1/3 Hz with pulse width of 50%, for the introduction of changes on the bottom floor (disturbances), as discussed in (Quanser, 2009a). By using the designed robust SDF controller, three cases were investigated, each one with a different mass M_s coupled in the active suspension system.

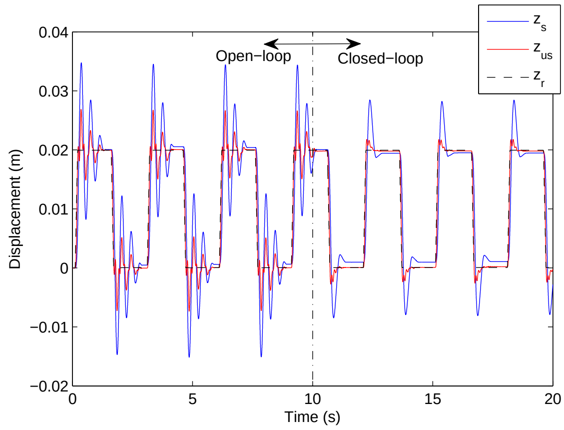

Figure 4: Open-loop and closed-loop responses for the system with $M_s = 2.45$ kg.

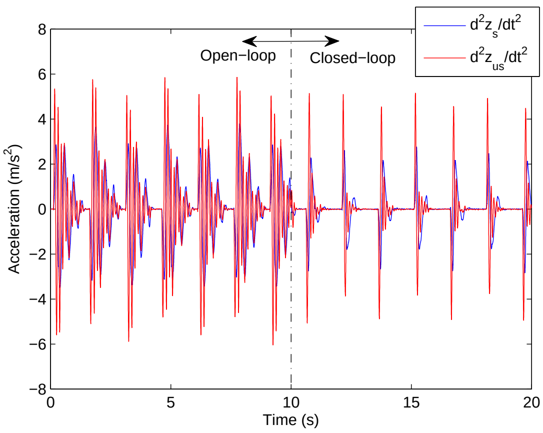

Figure 5: Open-loop and closed-loop responses of the accelerations for the active suspension system with total payload mass ($M_s = 2.45$ kg).

First, the two weight units were coupled in the active suspension system ($M_s = 2.45$ kg). Fig. 4 presents the resulting dynamic behavior of the system. A vertical dotted line indicates the time $t = 10$s when the control starts to operate (closed-loop). As can be seen, even in open-loop, the system is stable. However, without the control action, the displacements z_s and z_{us} of the masses M_s and M_{us} present large oscillations. By using the robust SDF controller, these oscillations were significantly reduced, as shown in the closed-loop responses, with the overshoot and settling time attenuated. Fig. 5 shows the filtered acceleration signals $\ddot{z}_s$ and $\ddot{z}_{us}$. The control signal effort for the active suspension system with total payload mass ($M_s = 2.45$ kg) is illustrated in Fig. 6.

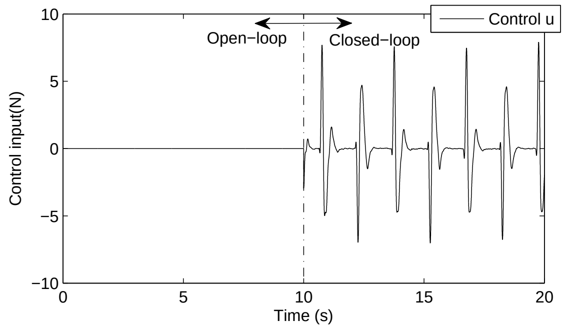

Figure 6: Control input for the system with $M_s = 2.45$ kg.

It is worth mentioning that the presence of offset in the displacement responses is due to nonlinearities that occur in the actual active suspension system, such as dry friction, which is not considered in the design model.

After removing a weight unit, the next test was implemented, for the system with half of the payload mass ($M_s = 1.9525$ kg). Fig. 7 and Fig. 8 show the displacements and accelerations of the system in this condition, respectively. Fig. 9 presents the corresponding control signal effort.

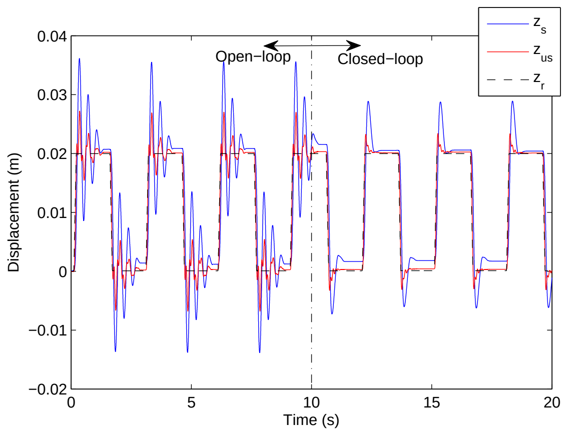

Figure 7: Open-loop and closed-loop responses for the system with $M_s = 1.9525$ kg.

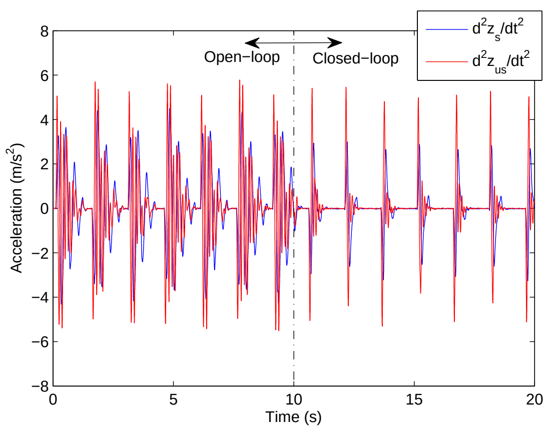

Figure 8: Open-loop and closed-loop responses of the accelerations for the active suspension system with half of the payload mass ($M_s = 1.9525$ kg).

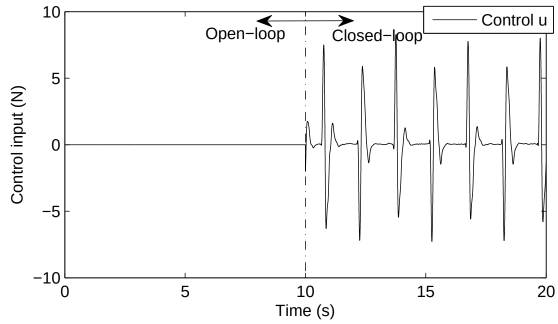

Figure 9: Control input for the system with $M_s = 1.9525$ kg.

Lastly, for the third implementation, the other weight unit was also removed, resulting in no payload mass coupled to the active suspension system ($M_s = 1.455$ kg). The dynamic behavior of the system without the payload mass is exhibited in Fig. 10 and Fig. 11. The corresponding control signal effort is shown in Fig. 12.

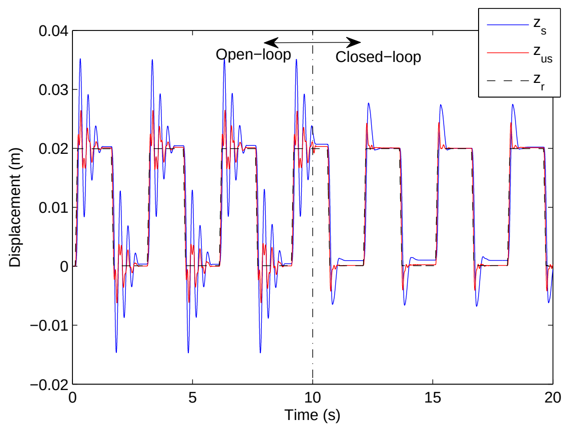

Figure 10: Open-loop and closed-loop responses for the system with $M_s = 1.455$ kg.

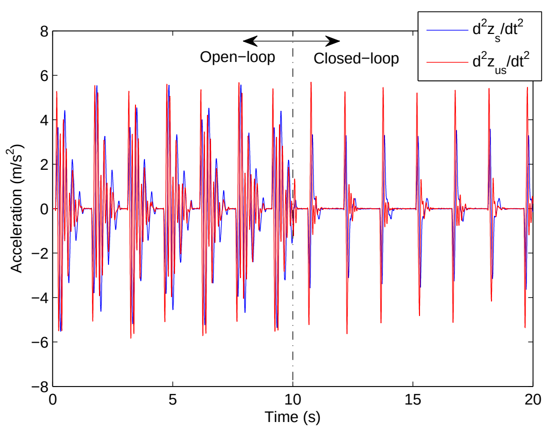

Figure 11: Open-loop and closed-loop responses of the accelerations for the active suspension system without payload mass ($M_s = 1.455$ kg).

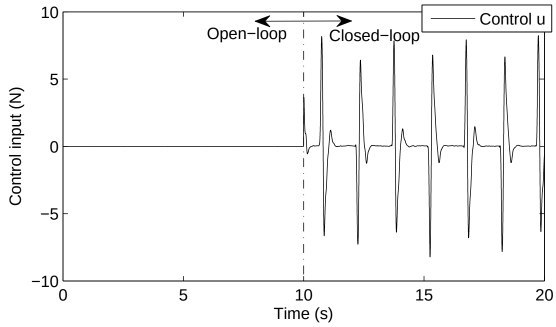

Figure 12: Control input for the system with $M_s = 1.455$ kg.

In this quarter car model, the acceleration $\ddot{z}_s$ of the sprung mass M_s can be a measure for the ride comfort, which is related to vehicle body motion sensed by the passengers (Quanser, 2009b). An analysis of the acceleration $\ddot{z}_s$ obtained for the system in open and closed loop, for different values of M_s, is shown in Table 2. As can be seen, in closed-loop, the acceleration was decreased compared to the open-loop response, which would result in a more comfortable ride for the passengers in an actual vehicle.

Table 2: Maximum absolute value and root mean square (RMS) value of the acceleration $\ddot{z}_s$ for the open and closed-loop system with different values of M_s.

M_s (kg)	Loop status	$max\|\ddot{z}_s\|$ (m/s^2)	$RMS[\ddot{z}_s(t)]$ (m/s^2)
2.45	Open	3.79	1.54
	Closed	2.84	0.75
1.9525	Open	4.49	1.77
	Closed	3.26	0.84
1.455	Open	5.57	2.05
	Closed	3.63	0.93

Thus, the designed SDF controller was able to improve the dynamic behavior of the active suspension system with robustness to the uncertainty in the mass M_s. For different values of M_s, within its range considered in the controller design, the closed-loop responses presented significant reduction of the oscillations caused by changes on the bottom floor z_r.

6 Conclusion

This paper presented a practical implementation of the robust discrete-time SDF control law proposed in (Rossi et al., 2018) in an active suspension system. By considering the measurements only from accelerometers and the presence of an uncertain mass of the vehicle body, an SDF controller was designed with robustness to parametric uncertainties using a state derivative design model. The control problem consisted of reducing the oscillations caused by changes on the bottom floor. The results exhibited that the designed SDF controller improved the dynamic behavior of the active suspension system, for different values of the uncertain mass. The use of filters to remove bias and high frequency noises from the signals measured by the accelerometers did not compromise the results. However, future investigations could be carried out to obtain explicit robustness with respect to the presence of the filters. Moreover, future implementations could be concerned with the active suspension system subject to input time delay or fault in the actuator.

Acknowledgments

The authors acknowledge the support of FAPESP (research grant 2011/17610-0) and CNPq (doctoral scholarship 140585/2014-1 and research fellowships 303714/2014-0, 310798/2014-0, 301227/2017-9).

References

Abdelaziz, T. H. S. (2012). Parametric eigenstructure assignment using state-derivative feedback for linear systems, *Journal of Vibration and Control* **18**(12): 1809–1827.

Abdelaziz, T. H. S. and Valášek, M. (2004). Pole-placement for SISO linear systems by state-derivative feedback, *IEE Proceedings - Control Theory and Applications* **151**(4): 377–385.

Assunção, E., Teixeira, M. C. M., Faria, F. A., da Silva, N. A. P. and Cardim, R. (2007). Robust state-derivative feedback LMI-based designs for multivariable linear systems, *International Journal of Control* **80**(8): 1260–1270.

Braga, M. F., Morais, C. F., Tognetti, E. S., Oliveira, R. C. L. F. and Peres, P. L. D. (2014). Discretization and control of polytopic systems with uncertain sampling rates and network-induced delays., *International Journal of Control* **87**(11): 2398–2411.

Cardim, R., Teixeira, M. C. M., Faria, F. A. and Assunção, E. (2009). LMI-based digital redesign of linear time invariant systems with state-derivative feedback, *In. Proc. IEEE Multi-Conf. Systems and Control, Saint Petersburg, Russia* pp. 745–749.

Chilali, M. and Gahinet, P. (1996). H_∞ design with pole placement constraints: An LMI approach, *IEEE Transactions on Automatic Control* **41**(3): 358–367.

da Silva, E. R. P., Assunção, E., Teixeira, M. C. M. and Buzachero, L. F. S. (2012). Less conservative control design for linear systems with polytopic uncertainties via state-derivative feedback, *Mathematical Problems in Engineering* **2012**(Article ID 315049).

da Silva, E. R. P., Assunção, E., Teixeira, M. C. M. and Cardim, R. (2013). Robust controller implementation via state-derivative feedback in an active suspension system subject to fault, *In Proc. Conf. Control Fault-Tolerant Syst., Nice, France* pp. 752–757.

Duan, Y. F., Ni, Y. Q. and Ko, J. M. (2005). State-derivative feedback control of cable vibration using semiactive magnetorheological dampers, *Computer-Aided Civil and Infrastructure Engineering* **20**(6): 431–449.

Fallah, S., Khajepour, A., Fidan, B., Chen, S. K. and Litkouhi, B. (2013). Vehicle optimal torque vectoring using state-derivative feedback and linear matrix inequalities, *IEEE Transactions on Vehicular Technology* **62**(4): 1540–1552.

Faria, F. A., Assunção, E., Teixeira, M. C. M. and Cardim, R. (2010). Robust state-derivative feedback LMI-based designs for linear descriptor systems, *Mathematical Problems in Engineering* **2010**(Article ID 927362).

Faria, F. A., Assunção, E., Teixeira, M. C. M., Cardim, R. and da Silva, N. A. P. (2009). Robust state-derivative pole placement LMI-based designs for linear systems, *International Journal of Control* **82**(1): 1–12.

Quanser (2009a). *Active Suspension - Instructor Manual*, Quanser Consulting Inc., Ontario, Canada.

Quanser (2009b). *Active Suspension - User Manual*, Quanser Consulting Inc., Ontario, Canada.

Reithmeier, E. and Leitmann, G. (2003). Robust vibration control of dynamical systems based on the derivative of the state, *Archive of Applied Mechanics* **72**(11-12): 856–864.

Rossi, F. Q. (2018). *Discrete-time design of control laws using state derivative feedback*, PhD thesis, Instituto Tecnológico de Aeronáutica, São José dos Campos, SP.

Rossi, F. Q., Galvão, R. K. H., Teixeira, M. C. M. and Assunção, E. (2018). Direct discrete time design of robust state derivative feedback control laws, *International Journal of Control* **91**(1): 70–84.

Rossi, F. Q., Teixeira, M. C. M., Galvão, R. K. H. and Assunção, E. (2013). Discrete-time design of state-derivative feedback control laws, *In Proc. Conf. Control Fault-Tolerant Syst., Nice, France* pp. 808–813.

Tseng, Y. W. and Hsieh, J. G. (2013). Optimal control for a family of systems in novel state derivative space form with experiment in a double inverted pendulum system, *Abstract and Applied Analysis* **2013**(Article ID 715026).

Yang, J. N., Li, Z. and Liu, S. C. (1991). Instantaneous optimal control with acceleration and velocity feedback, *Probabilistic Engineering Mechanics* **6**(3-4): 204–211.

A Regional Pole Placement (CHILALI; GAHINET, 1996)

Consider a discrete-time model of the form

$$x((k+1)T) = \Phi x(kT) + \Gamma u(kT), \tag{16}$$

where $x(kT) \in \mathbb{R}^n$, $u(kT) \in \mathbb{R}^m$ are the state and input vectors at time kT. Matrices (Φ, Γ) are assumed to belong to a polytope Ω with known vertices (Φ_i, Γ_i), $i = 1, 2, \ldots, N$.

Moreover, let $\mathcal{D}$ be a region in the complex plane described by

$$\mathcal{D} = \{z \in \mathbb{C} \mid \alpha + z\beta + \bar{z}\beta^T < 0\} \tag{17}$$

where $\bar{z}$ denotes the complex conjugate of z and α, β are $(p \times p)$ matrices of real-valued coefficients, with α symmetrical.

If there exist matrices $X = X^T \in \mathbb{R}^{n\times n}$ and $L \in \mathbb{R}^{m\times n}$ such that the following LMIs are satisfied (Chilali and Gahinet, 1996):

$$\begin{aligned} &\alpha \otimes X + \beta \otimes (\Phi_i X + \Gamma_i L) + \\ &\quad + \beta^T \otimes (\Phi_i X + \Gamma_i L)^T < 0,\ i = 1, \ldots, N \quad (18) \\ &X > 0 \quad (19) \end{aligned}$$

then a control law of the form $u(kT) = Fx(kT)$, with $F = LX^{-1}$, will place the closed loop poles inside $\mathcal{D}$, for any $(\Phi, \Gamma) \in \Omega$. The symbol $\otimes$ denotes the Kronecker product of matrices.

A particular case consists of placing the closed loop poles inside a circle of radius r and center $(\chi_0, 0)$, i.e. $\mathcal{D} = \{z = (\chi + j\nu) \mid (\chi - \chi_0)^2 + \nu^2 < r^2\}$. For this purpose, Schur's complement can be used to rewrite the inequality $(\chi - \chi_0)^2 + \nu^2 < r^2$ as

$$\begin{bmatrix} -r & -\chi_0 + z \\ -\chi_0 + \bar{z} & -r \end{bmatrix} < 0 \tag{20}$$

which can be cast into the form $\alpha + z\beta + \bar{z}\beta^T < 0$ of (17), with α and β given by (Rossi et al., 2018):

$$\alpha = \begin{bmatrix} -r & -\chi_0 \\ -\chi_0 & -r \end{bmatrix}, \quad \beta = \begin{bmatrix} 0 & 1 \\ 0 & 0 \end{bmatrix} \tag{21}$$